Sustainable Energy & Fuels

ROYAL SOCIETY OF CHEMISTRY

PAPER

View Article Online
View Journal | View Issue

Cite this: *Sustainable Energy Fuels*, 2023, 7, 4273

Enhancing the catalytic performance of Ni based catalysts in toluene reforming at low temperature by structuring on SiC extrudates†

Lole Jurado, ‡* Michaël Martin Romo y Morales, Sébastien Thomas and Anne-Cécile Roger

In biomass gasification, the use of metal-supported catalysts as primary catalysts for tar removal in an in-bed configuration is limited by their fast deactivation due to the generation of coke deposits. Pellets, rings, or monolithic structures are crucial to support the catalytic phase for its use as a secondary catalyst in a downstream reactor to increase the lifetime of the catalyst and diminish operational issues such as pressure drops. In the present work, catalytic structuration on SiC extrudates was conducted for a (Ru)Ni/perovskite ((Ru)Ni/LSCF). The influence of the catalytic structuration on the physicochemical properties of the catalysts was investigated using XRD, N_2 physisorption, H_2-TPR and SEM. Both powders and structured catalysts were pre-treated in a model ex-biomass gas atmosphere and subsequently tested in toluene reforming reaction at relatively low temperature (550 °C). Ni/LSCF$_{powder}$ was found to be inactive in toluene reforming, with the conversion being increased from <5% to 19% when adding Ru. An enhancement in the activity in toluene reforming was observed by structuration of the powders on SiC extrudates, increasing the conversion from <5% to 20% for Ni/LSCF and from 19% to 50% for RuNi/LSCF. This was ascribed to the strong metal–support interaction and the high resistance to coke deposition evidenced for the structured systems.

Received 29th May 2023
Accepted 16th July 2023

DOI: 10.1039/d3se00705g

rsc.li/sustainable-energy

1. Introduction

The formation of tars is one of the major concerns of biomass gasification processes.[1–3] Tars are a mixture of light and heavy hydrocarbons and oxygenated compounds that can easily condensate, causing several operational problems and water contamination.[2,3] These compounds can also limit the downstream applications of the syngas generated during biomass gasification processes. Among the several methods reported for tar removal, the use of a catalyst is widespread. The catalysts used for tar removal are generally classified in two groups: (i) primary (or in bed) and (ii) secondary catalysts. The former is directly added into the gasifier reactor together with the biomass feedstock, while the latter is commonly placed in a downstream catalytic reactor.[2–4] The design of the gasification pilot plant most of the time determines the type of catalyst required. The use of a fluidized-bed gasifier with an in-bed catalyst is the most effective configuration for tar removal in large installations (power generation > 2 MW).[3,5] In small installations (power generation < 1 MW), the downdraft fixed-bed gasifier seems to be the most widespread design.[3,5,6] Particles and ashes resulting from the gasification process are easily accumulated in the bottom of this type of gasifier, limiting the use of in-bed catalysts. According to Claude *et al.*,[3] the use of a secondary catalyst is the only route for cleaning and upgrading the raw syngas out from a fixed-bed gasifier.

Catalytic reforming of tars using nickel-based catalysts has been reported as the most efficient method for tar removal in the literature.[2,3,7,8] Two Ni-based catalysts using a perovskite ($La_{0.6}Sr_{0.4}Co_{0.2}Fe_{0.8}O_{3-\delta}$ (LSCF)) as a support have been previously prepared for their final use as secondary catalysts in a downdraft fixed-bed gasifier.[9] The synthesis was conducted *via* wetness impregnation (Ni/LSCF) and sol–gel synthesis (Ni–LSCF). After reduction in a H_2 atmosphere, the two Ni/perovskite catalysts were tested in tar reforming reaction at 550 °C using a model ex-biomass gas composition and toluene as one of the model tar molecules. Both the model ex-biomass gas composition and the inlet toluene content were selected based on the real gas composition obtained in a pilot plant fixed-bed gasifier set-up.[10] Although the same toluene conversion was found for both catalysts, the Ni/LSCF was more prone to form coke deposits than Ni–LSCF due to the acidic character of its surface.[9] The impregnation with a small amount of Ru over Ni/LSCF (RuNi/LSCF) was found to improve both its resistance to

Institute of Chemistry and Processes for Energy, Environment and Health, ECPM, UMR 7515, University of Strasbourg, 25 Rue Becquerel, F-67087 Strasbourg, France. E-mail: dolores.jurado@icmse.csic.es

† Electronic supplementary information (ESI) available. See DOI: https://doi.org/10.1039/d3se00705g

‡ Current affiliation: Instituto de Ciencia de Materiales de Sevilla, Centro Mixto Universidad de Sevilla-CSIC, Américo Vespucio 49, 41092 Sevilla, Spain.

coke and its catalytic activity in toluene reforming. Certainly, highly active Ni-based catalysts in tar removal under real operational conditions were evidenced, which make them promising candidates as secondary catalysts in biomass gasification processes. However, they required a pre-reduction to generate the active phase, which is commonly conducted under a H_2 atmosphere at the laboratory scale. The raw syngas produced during biomass gasification was extensively used as a reducing atmosphere in the 90's. It contains reducing gases, such as CO, CH_4 and H_2, which may efficiently substitute the use of pure H_2, being a cost-effective alternative.[11] Tanaka *et al.* performed a life test of an in-bed catalyst based on NiO/Al_2O_3 in a wood gasification process at 700 °C.[12] The XRD of the sample after the test revealed that NiO was reduced during the gasification process. Similar behavior was reported by Garcia *et al.*, evidencing the reduction of a Ni/Al catalyst when it was directly added in the gasifier.[11,13,14] This was associated with the reducing atmosphere formed by the thermal decomposition of biomass. Although the use of raw syngas was extensive for the reduction of the catalyst in the 90's, information about how this atmosphere influences the properties of the catalyst and its catalytic performance is still lacking.

For industrial uses, the structuration of these catalysts on pellets, monoliths, foams, or rings is highly required to mitigate the pressure drop, improve the mechanical resistance, and guarantee a uniform temperature distribution in the catalytic bed.[15,16] In the last few years, SiC has emerged as a competitive catalytic support or carrier material for reforming reactions owing to its chemical inertness, high mechanical strength, high mass transfer and thermal conductivity.[17–26] Nguyen *et al.*[17] compared the catalytic performance in dry reforming of methane (DRM) of Ni/SiC and Ni/Al_2O_3. A higher stability and resistance to coke formation for Ni/SiC than Ni/Al_2O_3 was found. Unlike the typical Ni/Mg–Al spinel, a uniform temperature distribution in the catalytic bed under coupling partial oxidation of methane (POM) and steam reforming of methane (SRM) was found for Ni/Al_2O_3–SiC foam monoliths.[20] This highlighted that the structuration of the catalyst on SiC foam enhanced the mass and heat transfer, alleviating the hot spots and cold zones respectively caused by the exothermicity of POM and endothermicity of SRM. The influence of the support on the catalytic performance of nickel-based catalysts in steam reforming of glycerol was investigated by Kim *et al.*[18] An acidic (Al_2O_3), a basic (CeO_2) and a neutral (SiC) support were used. The neutral properties of the SiC with respect to Al_2O_3 and CeO_2 made possible to avoid the concurrent side reactions, giving rise to a high catalytic stability and a low amount of coke deposits during steam reforming of glycerol. Moreover, owing to the inactivity of the SiC in the water gas shift (WGS) reaction, the syngas ratio reached for Ni/SiC was the most suitable for the Fischer–Tropsch synthesis. SiC has been used as a catalytic support for chemical looping dry reforming of benzene by Nam *et al.* using a lab scale fluidized bed reactor.[26] Recently, SiC-foam monoliths have also been reported as outstanding catalytic carrier on which a catalytic support and an active phase were deposited for dry reforming of biogas.[27,28]

Considering that a high catalytic performance was previously reached for powdered (Ru)Ni/LSCF systems after their pre-reduction in a H_2 atmosphere,[9] the present work focuses on the catalytic structuration of these catalysts using SiC as a catalytic carrier and the evaluation of their pre-treatment under a model ex-biomass atmosphere (CH_4, H_2O, CO_2, H_2 and CO). Toluene was identified as the major component formed during wood gasification conducted in a pilot plant equipped with a fixed bed downdraft gasifier at Offenburg University.[10] Therefore, the effects of the catalytic structuration and the pre-treatment atmosphere on their catalytic performance in toluene reforming were investigated. The SiC was used in the shape of an extrudate which allows an efficient thermal transfer linked to the combination of exothermic and endothermic reactions that may simultaneously occur under a raw syngas atmosphere out from the biomass gasification process. Moreover, it may provide high mechanical resistance and diminish the pressure drops in the downstream fixed-bed reactor.

2. Experimental

2.1. Preparation of powdered catalysts

The catalytic support, $La_{0.6}Sr_{0.4}Co_{0.2}Fe_{0.8}O_{3-\delta}$ (LSCF), was prepared by a sol–gel method using the metal acetates as starting salts. A scheme of the procedure, previously described in other work, is shown in Fig. 1, path 1.[9] The resin obtained from the sol–gel synthesis was subsequently calcined in a static air atmosphere at 800 °C for 6 h to form the perovskite mixed oxide ($LSCF_{fresh}$).

Active phases, Ni and Ru, were added by wetness impregnation as reported elsewhere.[9] A Ni loading of 10 wt% was added using an ethanolic solution of nickel(II) nitrate hexahydrate, giving rise to Ni/LSCF. A successive impregnation of Ru was conducted over Ni/LSCF using an ethanolic solution of ruthenium(III) acetylacetonate for preparing RuNi/LSCF with a Ru loading of 1.0 wt%. After each impregnation, the powders were calcined at 500 °C for 6 h in a static air atmosphere.

2.2. Catalytic structuration on SiC extrudates

2.2.1. Preparation of the La–Sr–Co–Fe (LSCF) precursor solution. The precursor solution was prepared through the sol–gel synthesis previously described (Fig. 1 (path 2)). The same procedure as for $LSCF_{fresh}$ was followed until the formation of the resin.[9] The resin was subsequently re-dissolved in a given volume of solvent to achieve a precursor solution with a cationic concentration of 0.60 $mol_{total\ cations}\ L_{solvent}^{-1}$

Owing to the high chemical affinity, propionic acid was widely used for the re-dissolution of the resin (mixed propionates) in the research group for conducting catalytic structuration on several carrier materials such as SiC foam, Al and Al_2O_3.[16,29,30] However, its corrosive properties and toxicity are some drawbacks of the use of this solvent for scaling up the catalytic preparation. In this work, water was used as a neutral and non-toxic solvent for re-dissolving the resin, being a greener alternative to propionic acid. To assess the impact of the dissolution on the physicochemical properties of LSCF, a given

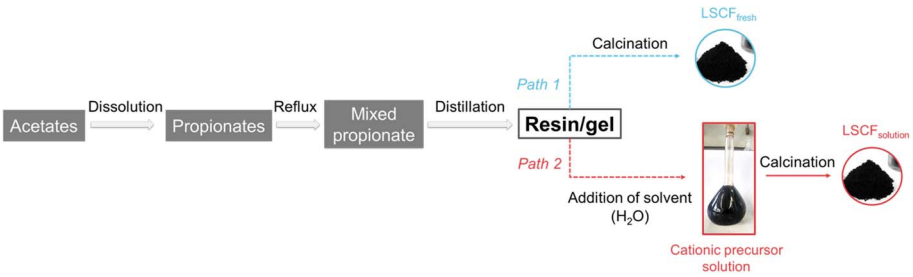

Fig. 1 Sol–gel synthesis of the powdered support (path 1) and the cationic precursor solution (path 2).

volume of the precursor solution ($LSCF_{solution}$) was calcined using the same thermal treatment as the one used for the preparation of $LSCF_{fresh}$ (800 °C for 6 h in static air atmosphere). The physicochemical properties of the resulting powder were compared with those of the fresh LSCF.

2.2.2. SiC extrudates. Open ring extrudates, mainly composed of β-SiC, were used as carrier materials. The main characteristics of the extrudates such as dimensions, packed density, or number of extrudates per liter are listed in Table 1. The extrudates displayed metallurgical purity as shown in the averaged elemental composition reported in Table 1S of the ESI.†

2.2.3. Dip coating procedure with the LSCF precursor solution. The coating procedure conducted is similar to the one described by Frey *et al.*[29] Small batches of 20–30 extrudates were coated with LSCF by dipping them for 2 min into the as-prepared precursor solution (Fig. 1S of the ESI†). After removing the excess of the solution by flashing them with compressed air, the extrudates were dried at 100 °C for 3 h and calcined in an air atmosphere using the same thermal treatment described above for $LSCF_{fresh}$ (800 °C for 6 h in static air atmosphere). The coated extrudates, LSCF/SiC, were exposed to an ultrasound bath for 5 min to evaluate the stability and anchoring of the LSCF phase at the surface of the SiC. This procedure was repeated until achieving an amount of 54 $g_{support}\ L_{ext}^{-1}$. As SiC is easily oxidized under air at 800 °C, forming a SiO_2–SiO_xC_y layer,[16,31,32] the mass uptake due to its oxidation was evaluated for the bare extrudates. To follow accurately the mass uptake resulting from the deposition of LSCF, the mass measured after each coating step was corrected by substracting the mass uptake from SiC oxidation.

The mass uptake ascribed to the deposition of LSCF measured after each coating step is shown in Fig. 2S(a) of the ESI† for three different batches. In general, a higher mass uptake of LSCF than the target one (54 $g_{support}\ L_{ext}^{-1}$) is reached after two coating steps, varying between 78 and 60 $g_{support}\ L_{ext}^{-1}$ among batches. This highlights that an accurate and reproducible deposition on SiC extrudates cannot be well achieved through the coating procedure used, being two coating steps, the minimum required to reach the target value. It has been reported that the air velocity used when blowing the excess of the solution out might influence the expected mass uptake or the coating load.[33] This could be one of the reasons of the differences found in the mass uptake of LSCF among the batches. The deposited mass remains stable after the ultrasound test (see Fig. 2S(a)†), indicating that a well anchored LSCF phase, due to a strong LSCF–SiC interaction, is achieved through the coating strategy followed.

2.2.4. Impregnation of the active phases. Active phases (Ni and Ru) were added on LSCF/SiC through the dip coating procedure described above (Fig. 1S of the ESI†) using nickel(II) nitrate hexahydrate and ruthenium(III) acetylacetonate as precursors. The coated extrudates, LSCF/SiC, were dipped for around 1 min in an ethanolic solution with a nickel(II) nitrate hexahydrate concentration of 0.26 M. Afterwards, the extrudates were dried at 100 °C for 3 h and subsequently calcined in a static air atmosphere at 500 °C for 6 h. The procedure was repeated until a Ni loading of 10 wt% was reached (6.0 $g_{Ni}\ L_{ext}^{-1}$), resulting in Ni/LSCF/SiC. An ethanolic solution with a ruthenium(III) acetylacetonate concentration of 0.050 M was used for adding 1 wt% of Ru on Ni/LSCF/SiC. After Ru impregnation, the extrudates were calcined using the same conditions as for Ni/LSCF/SiC (500 °C for 6 h in air). Ultrasound tests were conducted after each impregnation to evaluate the stability and anchoring of the active phases.

The mass uptake of Ni after two coating steps is also reported for three different batches in Fig. 2S(b) of the ESI.† The mass uptake exhibits a linear tendency, achieving around 4.0 and 1.7 g_{Ni} per L_{ext} per coating step for Ni/LSCF/SiC and RuNi/LSCF/SiC, respectively. As previously observed for LSCF deposition, the

Table 1 Main characteristics of β-SiC extrudates supplied by SICAT

Shape		$\varnothing_E$ (mm)	$\varnothing_I$ (mm)	Length (mm)	Packed density (g L^{-1})	No. extrudates per L
Ring		8	5	5	499	2.67×10^3

mass uptake of Ni varies among the batches. At least two impregnation steps are required for reaching a mass uptake (6.8 $g_{Ni}\ L_{ext}^{-1}$) close to the target one (6.0 $g_{Ni}\ L_{ext}^{-1}$) for Ni/LSCF/SiC, while rather low mass (4.0 $g_{Ni}\ L_{ext}^{-1}$) compared to the target one is obtained for the RuNi/LSCF/SiC. The differences in mass uptake of both, LSCF and Ni, led to structured catalysts with Ni loading ranging between 5 and 10% (see Table 2S of ESI†). The mass of Ni remains stable after the ultrasound test, suggesting that nickel also establishes strong interaction with the coated extrudates.

2.3. Characterization techniques

Textural properties such as specific surface area (SSA) and pore volume (V_{pore}) were determined through N_2 physisorption at 77 K on a Micromeritics sorptometer Tri Star 3000. Prior to the measurement, structured catalysts were ground into small pieces and both, powdered and structured catalysts, were outgassed at 250 °C for 3 h.

The crystalline structure was measured through X-ray diffraction (XRD) on a Bruker D8 Advance diffractometer with a LynxEve detector side and Ni filtered Cu K_α radiation. Diffractograms were collected in the 2θ range of 20–85° with a step of 0.050° and step time of 1.6 s. The structured catalysts were ground before the measurements.

The support reducibility and metal–support–SiC interaction were assessed by hydrogen temperature programmed reduction (H_2-TPR) on a Micromeritics AutoChem II equipped with a thermal conductivity detector (TCD). Around 50 mg of powdered or structured catalysts were heated up from RT to 950 °C in a 10 mol% H_2/Ar atmosphere with a total flow of 50 mL min^{-1} using a heating ramp of 15 °C min^{-1}. Before the analysis, the structured catalysts were ground. The H_2-TPR profiles normalized with respect to the mass of catalyst are plotted as a function of temperature. The support reducibility of each catalytic system has been estimated as follows:

$$\text{Reducibility } (\%) = \frac{n_{H_2,\text{exp}} - n_{H_2,(NiO,RuO_2)}}{n_{H_2,(Fe,Co)}} \times\ 100$$

where $n_{H_2,\text{exp}}$ is the experimental consumption of H_2 in mmol, $n_{H_2,(NiO,RuO_2)}$ is the mmol of H_2 required for fully reducing the nominal active metal content and $n_{H_2,(Fe,Co)}$ is the theoretical mmol of H_2 required to reduce all the reducing species present in the support, being Fe^{3+} and Co^{3+} in the case of LSCF.

The morphologies of the fresh catalysts deposited on SiC were evaluated by scanning electron microscopy (SEM) using a Zeiss GeminiSEM 500 microscope with an electron source based on the Schottky effect. After pre-treatment under a model ex-biomass gas atmosphere, the catalysts were also analyzed to determine the morphology of the carbon deposits formed at the surface.

The amount of the coke generated during toluene reforming reaction were determined by thermogravimetric analysis (TGA) on a Q5000 IR from TA instruments. Around 3 mg of spent catalysts were heated up from RT to 900 °C under air using a heating ramp of 10 °C min^{-1}. The amount of coke was reported as the mass of coke normalized by the mass of Ni introduced in the reactor ($g_{coke}\ g_{Ni}^{-1}$).

2.4. Catalytic tests

The catalytic tests were performed at atmospheric pressure in a fixed-bed down flow quartz reactor with an internal diameter of 5 mm in a homemade set up.[10] A scheme of the set-up is reported in Fig. 3S of the ESI.†

Prior to catalytic tests, the catalysts were submitted for *in situ* pre-treatment using a total gas flow (wet basis) of 139 N mL min^{-1} of a model ex-biomass gas atmosphere generated during wood gasification (2.8 N mL min^{-1} of CH_4, 13.9 N mL min^{-1} of H_2O, 16.7 N mL min^{-1} of CO_2, 22.2 N mL min^{-1} of H_2, 27.8 N mL min^{-1} of CO, balanced with N_2).[10] The catalytic bed was heated up from RT to 500 °C using a heating ramp of 5 °C min^{-1} and the temperature was held for 2 h. The possible modifications in the outlet gas composition during the *in situ* pre-treatment were measured using an on-line GC equipped with a TCD detector.

The catalytic tests were conducted under isothermal conditions at 550 °C for 6 h using the model ex-biomass gas atmosphere previously employed for the pre-treatment and an inlet toluene content of 13.4 g Nm^{-3} (toluene gas flow of 0.64 N mL min^{-1}). These reaction parameters were chosen based on the data from the wood gasification at the pilot plant scale downdraft gasifier at Offenburg University.[10] Due to the differences in Ni loading achieved through the structuration, the mass of Ni present in the reactor was kept constant (2.3 mg) for all the tests, leading to a $WHSV_{tar}$ of 26 h^{-1} (eqn (1)). Before being introduced into the reactor, the structured catalysts were crushed into small pieces, resulting in a catalytic bed with a height of around 1 cm.

$$\text{WHSV}_{\text{tar}}\ (\text{h}^{-1}) = \frac{\text{total tar mass flow}\ (\text{g h}^{-1})}{\text{mass of Ni (g)}} \qquad (1)$$

Two traps arranged in series were used for collecting the water, the unconverted toluene and condensable by-products that can be generated during the reforming reaction. The first trap was placed in an ice bath and the second one was placed in dry ice with acetone. The outlet partial molar flow of the gaseous components *versus* time, the average toluene conversion ($X_{toluene}$), the average benzene selectivity ($S_{benzene}$) and the amount of coke ($g_{coke}\ g_{Ni}^{-1}$) are reported for all the systems of this study. These parameters and their calculations have been described in our previous studies[9,10].

The carbon balance varied between 0.95 and 0.99 and it was estimated for each catalytic test as follow:

$$C = \frac{n_{C,\text{out}}}{n_{C,\text{in}}} = \frac{\sum_i F_{i,\text{out}}\Delta t_i + n_{C,\text{tol,out}} + n_{C,\text{coke}}}{\sum_i F_{i,\text{in}} t_i + n_{C,\text{tol,in}}},$$

where $n_{C,in}$ and $n_{C,out}$ are the total mmol of carbon at the inlet and outlet, respectively; $F_{i,in}$ is the inlet C1 gas flow (CO, CO_2 and CH_4) in mmol min^{-1}; ti is the time on stream (360 min), nC,tol,in is the inlet mmol of carbon from toluene; $F_{i,out}$ is the

C1 (CO, CO_2 and CH_4) gas flow in mmol min^{-1} measured in each sampling; Δt_i is the time interval in which the sampling was performed; nC,tol,out is the mmol of carbon from unconverted toluene and $n_{C,coke}$ is the mmol of carbon from the coke deposits measured by TGA.

3. Results and discussion

3.1. Characterization of the precursor solution

The specific surface area (SSA) and pore volume (V_{pore}) of the supports formed after the calcination of the resin ($LSCF_{fresh}$) and precursor solution ($LSCF_{solution}$) are reported in Table 2. Similar values were found for both materials, suggesting that the re-dissolution of the resin in water does not influence the textural properties of the final perovskite. Low SSA (7–8 $m^2\ g^{-1}$) and pore volume (0.02–0.04 $m^2\ g^{-1}$) were observed, due to the high calcination temperature required for the formation of the perovskite.

Diffractograms of the supports are shown in Fig. 2(a). As previously reported, a perovskite structure with orthorhombic symmetry ($La_{0.7}Sr_{0.3}Fe_{0.7}Co_{0.3}O_{3-\delta}$, JPCD 01-089-1268) as the predominant phase and lanthanum oxide (La_2O_3, JPCD 01-083-1344), as the secondary phase, were observed for $LSCF_{fresh}$.[9] An additional perovskite phase with hexagonal symmetry ($La_{0.85}Sr_{0.15}CoO_{3-\delta}$, JPCD 01-153-3518) is observed for $LSCF_{solution}$ (Fig. 2(a), inset). Most likely the re-dissolution causes the partial hydrolysis of the resin, favoring the formation of this new phase. The shift to higher 2θ of the $LSCF_{solution}$ diffraction peaks when compared with $LSCF_{fresh}$ evidences the contraction of the lattice. It could be associated with the incomplete insertion of La/Sr in the LSCF structure due to the formation of the new perovskite phase generated by the re-dissolution.

The crystalline size ($d_{support}$) and support lattice parameters ($a_{support}$) of the supports are listed in Table 2. The crystalline sizes were calculated using the Scherrer equation, while lattice parameters were calculated by assuming a pseudo-cubic structure.[9] The crystalline sizes are not modified after the re-dissolution of the resin, found to be around 17–18 nm. As expected from the shift in its diffraction peaks (Fig. 2(a)), a smaller lattice parameter is attained for the $LSCF_{solution}$ (3.84 Å) with respect to the $LSCF_{fresh}$ one (3.87 Å). This decrease might be ascribed to a lower La/Sr content into the LSCF structure as a consequence of the formation of the new $La_{0.85}Sr_{0.15}CoO_{3-\delta}$ phase.

Two reduction regions are clearly distinguished in the H_2-TPR profiles of the supports (Fig. 2(b)). The first one at temperatures below 500 °C (region I) has been ascribed to the reduction process of Co^{3+} cations, while the one at temperature above 500 °C (region II) has been linked to the reduction of Fe^{3+} species.[9] By comparison with $LSCF_{fresh}$, the re-dissolution of the resin leads to some modifications in the reduction profiles of $LSCF_{solution}$. Some new peaks emerge for $LSCF_{solution}$ in region I, giving rise to a barely different shape in comparison with $LSCF_{fresh}$. It has been reported that the reducibility of Co species is widely affected by the chemical environment such as location and coordination number into the structure,[34] with the reduction temperature of these species being structurally sensitive.

Table 2 Physicochemical properties of supports from resin ($LSCF_{fresh}$) and precursor solution ($LSCF_{solution}$). Data for the support from resin were taken from ref. 9

	SSA ($m^2\ g^{-1}$)	V_{pore} ($cm^3\ g^{-1}$)	$d_{support}$ (nm)	$a_{support}$ (Å)	Reducibility (%)
$LSCF_{fresh}$	7	0.04	17	3.87	29
$LSCF_{solution}$	8	0.02	18	3.84	31

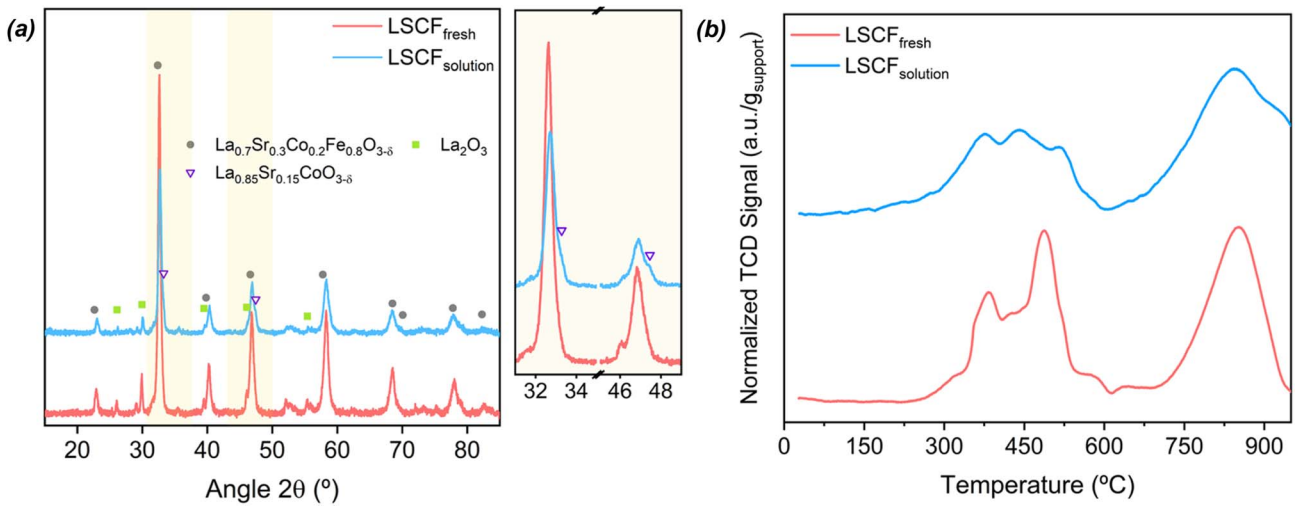

Fig. 2 (a) Diffractograms and (b) H_2-TPR profiles of supports obtained from the resin ($LSCF_{fresh}$) and from the precursor solution ($LSCF_{solution}$). Data for the support from resin were taken from ref. 9.

Therefore, it could be assumed that the chemical environment of the Co species in the LSCF structure changed after the re-dissolution of the resin. The formation of a secondary perovskite after the re-dissolution ($La_{0.85}Sr_{0.15}CoO_{3-\delta}$), confirmed by XRD, might cause these changes in the reduction temperature and shape. In contrast to $LSCF_{fresh}$, two reduction peaks are displayed for $LSCF_{solution}$ in region II, most likely ascribed to the reduction of $Fe^{4+/3+}$ into $Fe^{3+/2+}$.[35] However, it is rather difficult to clarify the different reduction processes that may occur due to the complex composition of these materials. The support reducibility (Table 2) was estimated by considering only Co/Fe as the reducible species in the perovskite structure. Although the re-dissolution of the resin affects the reduction processes, modifying the chemical environment, it does not influence the support reducibility (~30%).

3.2. Characterization results

Diffractograms of the powders and structured catalysts are presented in Fig. 3. A perovskite with orthorhombic symmetry ($La_{0.7}Sr_{0.3}Co_{0.3}Fe_{0.7}O_{3-\delta}$, JPCD 01-089-1268) remains as the main phase for $Ni/LSCF_{powder}$ (Fig. 3(a)). The formation of $LaNiO_3$, evidenced for $Ni/LSCF_{powder}$ in a previous study, explains the absence of La_2O_3 and NiO in its diffractogram.[9] These crystalline phases are modified after the catalytic structuration. Reflection peaks mainly associated with β-SiC (JPCD 00-101-0995) are evidenced for the bare SiC (Fig. 3(b)). The small peak at 33.5° evidences the formation of α-SiC caused by the presence of stacking faults in the (111) reticular plane.[36] Only reflection peaks with low relative intensity ascribed to La_2O_3 are observed for LSCF/SiC. This might be due to the hydrolysis of the resin during its re-dissolution, suggesting that the formation of the individual oxides prevails over the perovskite mixed oxide for the structured catalysts. The intensity of the reflection peak related to La_2O_3 decreases for Ni/LSCF/SiC (Fig. 3(b), inset). This fact might denote the generation of $LaNiO_3$ after Ni impregnation, as it has been shown for $Ni/LSCF_{powder}$. Additional reflection peaks at 44 and 62° linked to a cubic NiO phase (JPCD 03-065-2901) are observed for Ni/LSCF/SiC.

A comparison between the H_2-TPR profiles of powders (dotted lines) and structured (solid lines) catalysts is shown in Fig. 4(a). The TPR of the powders shows two reduction regions, previously ascribed to the reduction of the Co (region I) and Fe (region II) species.[9] The reduction of the Ni species, existing as $LaNiO_3$ in the $(Ru)Ni/LSCF_{powder}$, and the reduction of Co species can simultaneously occur in region I.[9,37] An additional reduction peak at low temperature is observed for both $Ni/LSCF_{powder}$ and $RuNi/LSCF_{powder}$, which have been respectively linked to the reduction of NiO and RuO_2 having a weak metal–support interaction.[9]

The structuration leads to some changes in the reduction profiles in terms of the shape and reduction temperature by comparison with the powders. The same as for $LSCF_{solution}$, two regions are also found for LSCF/SiC. Region I shows a simpler shape for LSCF/SiC than for $LSCF_{solution}$, indicating that the structuration slightly modifies the phases formed on the SiC. According to the XRD results (Fig. 3(b)), it may be difficult to generate the perovskite mixed oxide ($La_{0.6}Sr_{0.4}Co_{0.2}Fe_{0.8}O_{3-\delta}$), since the re-dissolution of the resin causes its hydrolysis, facilitating the formation of the individual oxides. A single peak centered at 620 °C for LSCF/SiC is observed in region I and a main reduction peak is shown at 830 °C in region II. Reduction peaks of the Co_3O_4 in weak interaction with the SiC are reported at temperatures around 300–400 °C.[38,39] According to Díaz *et al.*, reducible cobalt silicate, as a consequence of a strong Co–SiC interaction, could also be formed, being reduced at 600 °C.[39] The temperature required for reducing the Co species in LSCF/SiC suggests the formation of Co_3O_4 species in strong interaction with the SiC or the formation of cobalt silicates. The peak at 830 °C is ascribed to the reduction of Fe species. Both regions are shifted to higher temperatures for LSCF/SiC than $LSCF_{solution}$, indicating that a strong LSCF–SiC interaction is accomplished through the structuration. This fact explains the negligible mass loss previously observed after the ultrasound test.

Two reduction regions are also observed for Ni/LSCF/SiC. Although the NiO phase was observed by XRD for Ni/LSCF/SiC (Fig. 3(b)), the reduction peak at 270 °C displayed for $Ni/LSCF_{powder}$, linked to NiO species in weak interaction with the LSCF, is no longer observed for the structured catalyst. It might be possible that NiO species in strong interaction with the SiC are favored through the catalytic structuration. The same as for

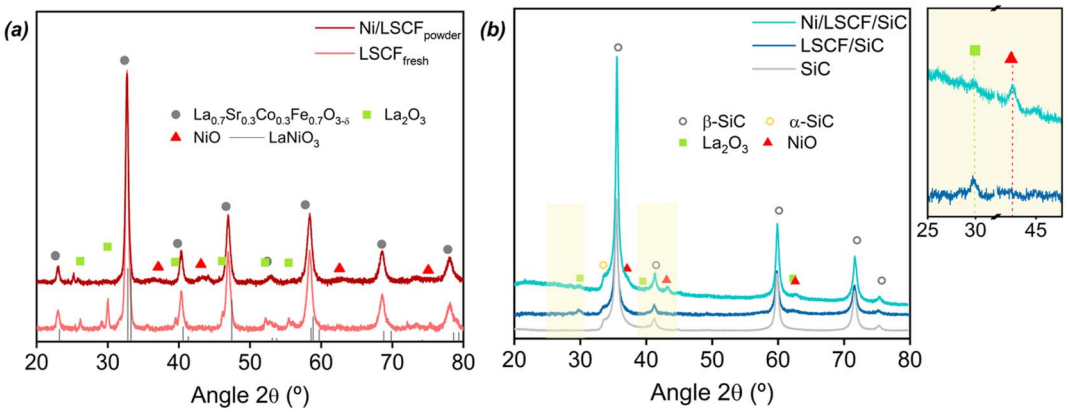

Fig. 3 Diffractograms of (a) powdered and (b) structured catalysts. (Data for the powders were taken from ref. 9.)

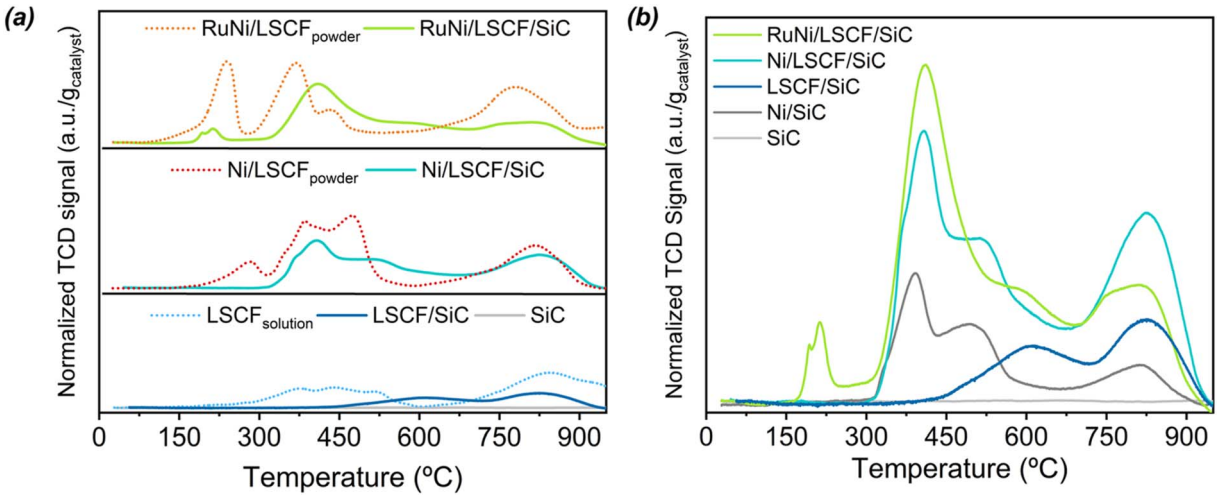

Fig. 4 H_2-TPR profiles of (a) powders and structured LSCF and (b) structured catalysts. (Data for the powders were taken from ref. 9.)

RuNi/LSCF$_{powder}$, a small reduction peak is observed at low temperature for RuNi/LSCF/SiC, ascribed to the reduction of RuO_2.[9] The shift of region I to higher temperature for RuNi/LSCF/SiC than for RuNi/LSCF$_{powder}$ indicates, once again, that phases having a strong interaction with the SiC are formed for the structured catalysts.

In order to identify the Ni species generated through the structuration, Ni was directly impregnated on SiC extrudates (Ni/SiC), following the same coating procedure as previously described. The H_2-TPR profiles of the Ni/SiC and structured catalysts are reported in Fig. 4(b). Three characteristic peaks can be distinguished in the reduction profile of Ni/SiC. The first two are partially overlapped and placed at relatively low temperature (350 and 500 °C), while the third one is found at high temperature (830 °C). The peak at 350 °C has been widely related to the reduction of bulk NiO having a weak interaction with SiC,[21,40–44] while the assignment of the peaks shown at higher temperatures (500 and 830 °C) is debated. Reduction peaks at 620 and 820 °C associated with the thermal decomposition of layered Ni silicates were observed for Ni/SiO_2.[45] Three reduction peaks at temperatures around 400, 560 and 700 °C were reported for Ni/SiO_2 catalysts with different Ni loadings.[41] The peaks at 400 and 560 °C were respectively ascribed to the reduction of NiO species having a weak and strong interaction with the SiO_2, whereas the peak at temperatures higher than 700 °C was ascribed to the reduction of nickel silicates. This peak placed at high temperature (>700 °C) has also been associated with the reduction of the nickel silicate in other studies.[21,42] Therefore, the reduction peak at 500 °C observed for Ni/SiC might be attributed to NiO species having a strong interaction with the SiC and the one shown at 830 °C might be linked to the reduction of nickel silicates. The same reduction peaks as for Ni/SiC are distinguished for Ni/LSCF/SiC, indicating that LSCF does not fully cover the SiC surface, with part of the NiO species being in close interaction with the SiC. The H_2 consumption observed between 500 and 650 °C for Ni/LSCF/SiC is related to the reduction of LSCF. Thus, NiO species having weak and strong interaction with the SiC and nickel silicate are also formed after Ni impregnation on the LSCF/SiC. The reduction profile slightly changes when Ru is added. The RuNi/LSCF/SiC material no longer exhibits the reduction peak at 500 °C, showing only one broad reduction peak in the temperature range of 300–500 °C. This fact could suggest that a strong Ru–Ni interaction is attained, favoring the reduction of NiO species with strong Ni–SiC interaction. The higher H_2 consumption achieved for RuNi/LSCF/SiC than for Ni/LSCF/SiC in the temperature range between 300 and 500 °C clearly evidences that the presence of Ru promotes the reduction of NiO.

The support reducibility of the powders and structured catalysts is reported in Table 2S of the ESI.† Regarding the powders, the addition of Ni on LSCF improved the support reducibility, increasing from 31% for LSCF$_{solution}$ to 54% for Ni/LSCF$_{powder}$. The same support reducibility as for Ni/LSCF$_{powder}$ is found after the addition of Ru (56% for RuNi/LSCF$_{powder}$). As previously reported, the addition of Ru favored the reduction of Ni, but did not affect the support reducibility.[9] The structuration leads to a severe decrease in the H_2 consumption, found to be around three times lower for LSCF/SiC (1.4 mmol $g_{catalyst}^{-1}$) than for LSCF$_{solution}$ (4.4 mmol $g_{catalyst}^{-1}$). Consequently, the support reducibility decreases from 30% to 10% when the LSCF is deposited on the SiC (Table 2S†). As the XRD and H_2-TPR results suggest, the structuration most likely led to the formation of other phases, *i.e.*, individual oxides or cobalt silicate, which display lower reducibility than the perovskite mixed oxide. As expected, the support reducibility of structured catalysts increases by adding Ni (~40% for Ni/LSCF/SiC), being slightly lower than the value found for the Ni/LSCF$_{powder}$ (~55%). The same support reducibility as for Ni/LSCF/SiC is displayed for RuNi/LSCF/SiC (~40%). This indicates that the addition of Ru only promotes the reduction of NiO, as it was observed for the powders.[9] This fact is in good agreement with the increase in the H_2 consumption observed in the TPR profile of RuNi/LSCF/SiC at low temperature (300–500 °C) (Fig. 4(b)), mainly ascribed to the reduction of the NiO species. Although a decrease in the support reducibility is achieved through the structuration due to the formation of different phases, the

behavior of the structured catalysts is similar to that of the corresponding powders.

SEM images of the powdered LSCF ($LSCF_{solution}$) and structured catalysts are reported in Fig. 5. Due to the high calcination temperature used, spherical and non-porous particles are found for the $LSCF_{solution}$ (Fig. 5(a)). Particles with similar morphology to the powdered LSCF are shown for LSCF/SiC (bright zones of Fig. 5(b)). Another kind of morphology, like a spider web, is exhibited for the deposited LSCF on SiC (Fig. 5(c)). Elements such as Sr, Co and Fe are found for LSCF/SiC by EDX analysis, reported in Fig. 5S of the ESI.† The presence of these elements, which were not previously observed by XRD (Fig. 3(b)), indicates that individual oxides are likely formed through the structuration. The impregnation of Ni over LSCF/SiC does not modify the morphology of the LSCF deposited, as shown in the bright zones in Fig. 5(d). The presence of Ni and the elements from LSCF (La, Sr, Co and Fe) are observed in the bright zones of Ni/LSCF/SiC (A1 and A3, Fig. 6S†), while Ni is no longer observed in the dark zones (A2 and A4, Fig. 6S†). This suggests that a heterogeneous dispersion of Ni over LSCF/SiC is attained. Rather big particles with "spherical" (Fig. 5(e)) and flower morphology (Fig. 5(f)) are observed for RuNi/LSCF/SiC. The bright particles are related to Ru (A1–A3, Fig. 7S†) and the flowers are ascribed to Ni (A1 and A2, Fig. 8S†). Although some elements linked to LSCF are shown in the EDX analyses for RuNi/LSCF/SiC (A3, Fig. 8S†), part of the Ru and Ni seems to be in direct contact with the SiC, being consistent with the TPR results already discussed.

3.3. *In situ* pre-treatment under a model ex-biomass atmosphere

The molar flow of each gaseous compound at the inlet and outlet of the reactor during the pre-treatment of the catalysts under model ex-biomass gas is reported in Fig. 6 for the powders (dotted lines) and structured catalysts (solid lines). All the catalysts show a strong consumption of CO with a simultaneous production of CO_2 and CH_4 at temperatures around 270–360 °C. Although the evolution of these molar flows might suggest that water gas shift (WGS, $CO + H_2O \leftrightarrow H_2 + CO_2$; $\Delta H^{\circ}_{298} = -41$ kJ mol^{-1}) and/or CO methanation ($CO + 3H_2 \leftrightarrow CH_4 + H_2O$; $\Delta_r H^{\circ}_{298\ K} = -206$ kJ mol^{-1}) simultaneously occur, a stable catalytic surface could not be reached due to the short time on stream. Therefore, additional tests to explain the occurrence of these reactions and draw more accurate conclusions are required. Despite that, the noteworthy variation of the outlet partial molar flows displayed for all the materials indicates that the reduction of NiO under these pre-treatment conditions is successfully achieved.

After the pre-treatment, the presence of carbonaceous deposits is found on the surface of both $Ni/LSCF_{powder}$ (Fig. 7(a)) and Ni/LSFC/SiC (Fig. 7(c)), while only perovskite particles were previously observed for the fresh ones (Fig. 5). Filamentous carbons such as carbon nanofibers (CNFs) or carbon nanotubes (CNTs) are mainly generated at the catalytic surface after the pre-treatment in a model ex-biomass gas atmosphere. The presence of the Ni particles on the top of the filamentous carbon is evidenced for the $Ni/LSCF_{powder}$ when the chemical contrast mode in the SEM analysis is used (Fig. 7(b)). This type of coke, well known as whisker carbon, is usually formed at reaction temperatures above 450 °C and, according to the literature, they are mainly formed through the Boudouard reaction or decomposition of methane or light hydrocarbons.[46] These filaments appear to cover the surface of the LSCF particles (bright zones) and the SiC (dark zones) for Ni/LSCF/SiC (Fig. 7(d)). Therefore, it

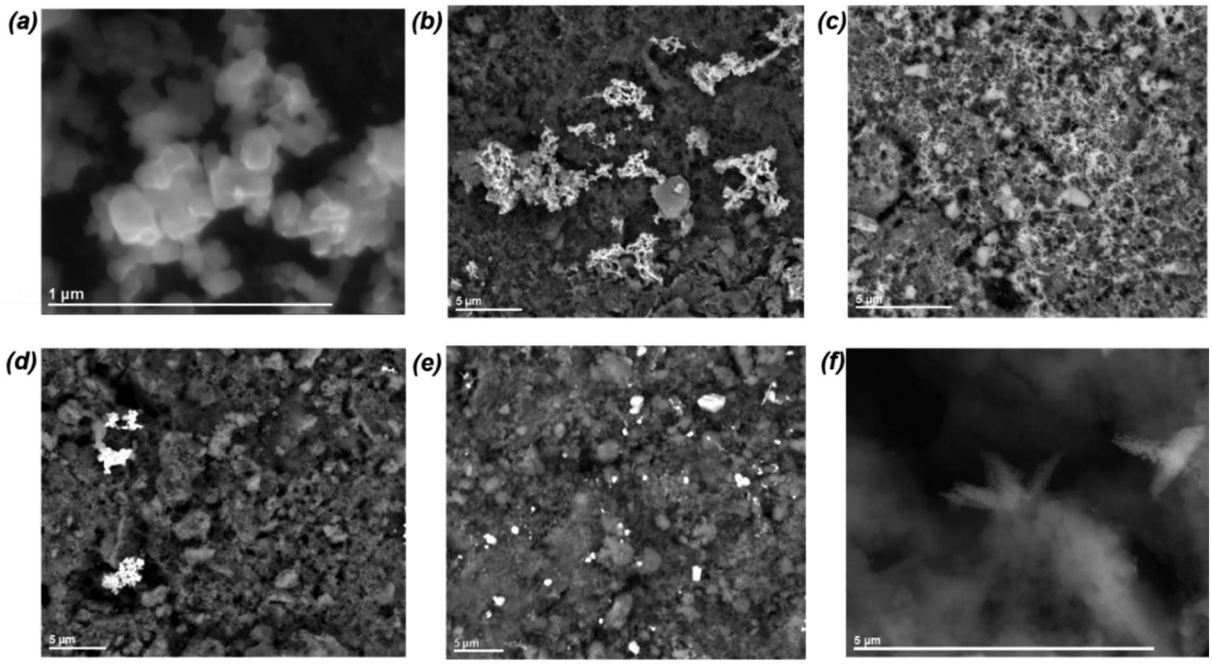

Fig. 5 SEM images of (a) $LSCF_{solution}$, (b and c) LSCF/SiC, (d) Ni/LSCF/SiC and (e and f) RuNi/LSCF/SiC.

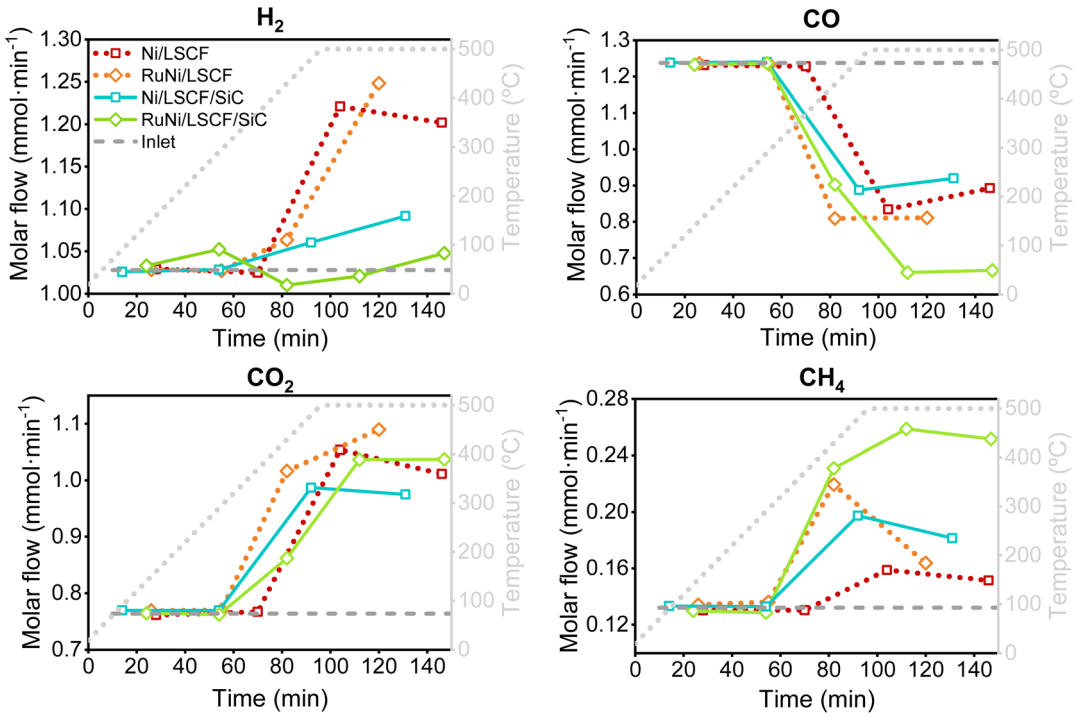

Fig. 6 Molar flows of gaseous components at the inlet and outlet of the reactor during the pre-treatment under a model ex-biomass atmosphere.

seems that the migration of the Ni at the top of the filaments is inhibited when the catalyst is deposited on SiC. Two growth mechanisms of these carbonaceous deposits were widely described in the literature for the Ni-based catalysts: (i) the base-growth and (ii) the tip-growth mechanism.[47] In the former one, the metal particle remains attached to the support, whereas these particles lift off the surface and placed at the top of the carbon nanotubes or filaments in the later.[47] The type of growth mechanism is closely related to the metal–support interaction, with the base growth being highly encouraged when the interaction is strong and the tip-growth when it is weak.[48,49] The use of a model ex-biomass gas atmosphere

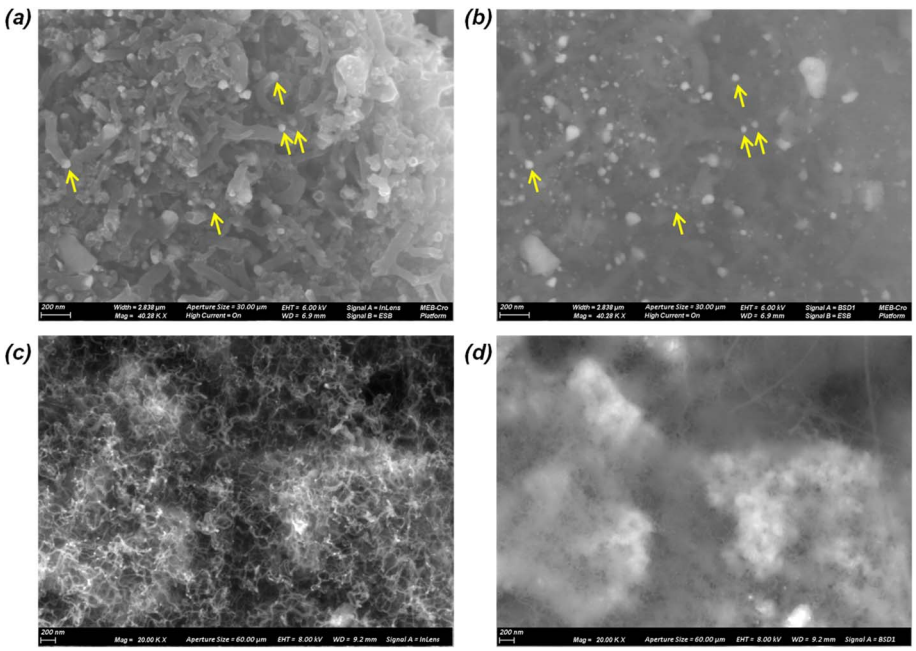

Fig. 7 SEM images with topological (right) and chemical (left) contrast of (a and b) Ni/LSCF$_{powder}$ and (c and d) Ni/LSCF/SiC.

respectively promotes the tip- and base-growth mechanisms of the carbon deposits for Ni/LSCF$_{powder}$ and Ni/LSCF/SiC. This indicates that the strength of the Ni–support interaction is modified by the catalytic structuration, becoming stronger than for the powders. This fact is in accordance with the TPR results previously discussed, in which the presence of NiO species having a strong interaction with the SiC and the formation of Ni silicates were evidenced for Ni/LSCF/SiC.

The nature as well as the amount of coke deposits generated during this pre-treatment have been evaluated by TGA for one of the powders (Ni/LSCF). The derivative of the TGA curve *versus* the temperature is reported in Fig. 4S of the ESI† for Ni/LSCF$_{powder}$. An amount of coke of 0.064 g_{coke} g_{Ni}^{-1} was found for Ni/LSCF$_{powder}$, with the oxidation temperature of these deposits being 480 °C. Several studies have reported the relationship between the nature of the carbon deposits and their oxidation temperature. It has been observed that amorphous carbon deposits are easily oxidized at relatively low temperatures (<500 °C), whereas carbon allotropes such as filamentous carbon (CNFs) or carbon nanotubes (CNTs) need higher oxidation temperatures (500–600 °C) since they are more stable than the amorphous one.[50–53] The graphitic or structural carbon, such as graphite, is usually oxidized at temperatures between 600 and 800 °C.[51] As can be seen in Fig. 4S of ESI,† an oxidation temperature of 480 °C is required to oxidize the carbonaceous species formed at the surface of both materials. This elucidates the generation of CNFs or CNTs with an amorphous character after pre-treatment in a model ex-biomass gas atmosphere, being in good agreement with the morphology found by SEM (Fig. 7).

3.4. Catalytic activity in toluene reforming

The catalysts pre-treated under model ex-biomass gas were tested in the toluene reforming reaction at relatively low temperature to investigate the effect of the catalytic structuration and the pre-treatment on the catalytic performance.

The average toluene conversion, the selectivity to benzene and the amount of coke deposited at the catalytic surface normalized by the mass of nickel (g_{coke} g_{Ni}^{-1}) are reported in Table 3. As is shown, Ni/LSCF is not efficient in tar removal, reaching an average toluene conversion close to zero and a relatively high amount of coke deposits (21 g_{coke} g_{Ni}^{-1}). Ruthenium slightly improves the catalytic activity in toluene reforming and the resistance to coke deposits of the bare Ni/LSCF. Thus, an average toluene conversion of 19% and a decrease by a factor of 2 in the amount of coke deposits (10 g_{coke} g_{Ni}^{-1}) are found for RuNi/LSCF. However, the selectivity to benzene increases when Ru is added, found to be quite high (10%). An improvement in the performance in toluene reforming is observed for the structured catalysts when compared with the powders. The average toluene conversion increases from less than 5 for Ni/LSCF to 22% for Ni/LSCF/SiC and the amount of coke decreases from 21 g_{coke} g_{Ni}^{-1} for Ni/LSCF to 5 g_{coke} g_{Ni}^{-1} for Ni/LSCF/SiC. A selectivity to benzene close to 10% is shown for Ni/LSCF/SiC. The same as for the powders, the addition of Ru on Ni/LSCF/SiC enhances the catalytic activity in toluene reforming, reaching the highest toluene conversion (55%). The amount of coke slightly increases for RuNi/LSCF/SiC (16 g_{coke} g_{Ni}^{-1}) compared to Ni/LSCF/SiC (5 g_{coke} g_{Ni}^{-1}) and RuNi/LSCF (10 g_{coke} g_{Ni}^{-1}). This increase in the coke deposits is in concordance with the relatively high activity in toluene reforming displayed for the RuNi/LSCF/SiC. Moreover, a decrease in the selectivity to benzene is also observed when RuNi/LSCF is structured, reaching a value of 4% for RuNi/LSCF/SiC.

The variations of the molar flow of the gaseous components (H_2, CO, CO_2 and CH_4) *versus* the time are plotted in Fig. 8 for the powders (dotted lines) and structured catalysts (solid lines). The impact of steam reforming reaction on the changes in the outlet C1 gas flows could be considered negligible due to the rather low inlet gas flow of tar injected (0.19 $mmol_C$ min^{-1}) with respect to the total inlet carbon (2.33 mmol min^{-1}). Both powders, Ni/LSCF and RuNi/LSCF, display a strong consumption of CO and a simultaneous production of H_2 and CO_2, with the production of CH_4 being negligible. This indicates that both catalysts show relatively high catalytic activity in the WGS reaction, while they are rather inactive in CO methanation. This behavior has been previously observed for these materials under the same reaction conditions using H_2 as a pre-treatment atmosphere. Their relatively high catalytic activity in WGS was linked to the high content of Sr found by XPS at their surface, which favored the water adsorption and promoted the WGS reaction.[9] The extremely low production of H_2 and CO_2 shown for Ni/LSCF/SiC evidences the lower activity in the WGS reaction of the Ni/LSCF/SiC than Ni/LSCF. The structuration of RuNi/LSCF on SiC also modifies the catalytic performance of the powder. The production of CH_4 and the consumption of CO attained at the first 150 min of the test for RuNi/LSCF/SiC suggest that CO methanation prevails over WGS. The activity of a given catalyst in WGS or CO methanation is widely governed by several factors such as particle size, catalytic support and/or reaction conditions.[54] As aforementioned, the structuration leads to some changes in the phases deposited, generating individual oxides as well as cobalt and nickel silicates, which

Table 3 Reaction conditions, average toluene conversion, selectivity to benzene and mass of coke deposits per mass of nickel during toluene reforming at 550 °C for 6 h

	m_{cata} (mg)	m_{Ni} (mg)	$WHSV_{gas}$ (h^{-1})	$WHSV_{tar}$ (h^{-1})	$X_{toluene}$ (%)	$S_{benzene}$ (%)	g_{coke} g_{Ni}^{-1}
Ni/LSCF	23	2.3	370	26	<5	—	21
RuNi/LSCF	23	2.3	370	26	19	10	10
Ni/LSCF/SiC	32	2.5	270	24	22	7	5
RuNi/LSCF/SiC	42	2.1	203	28	55	4	16

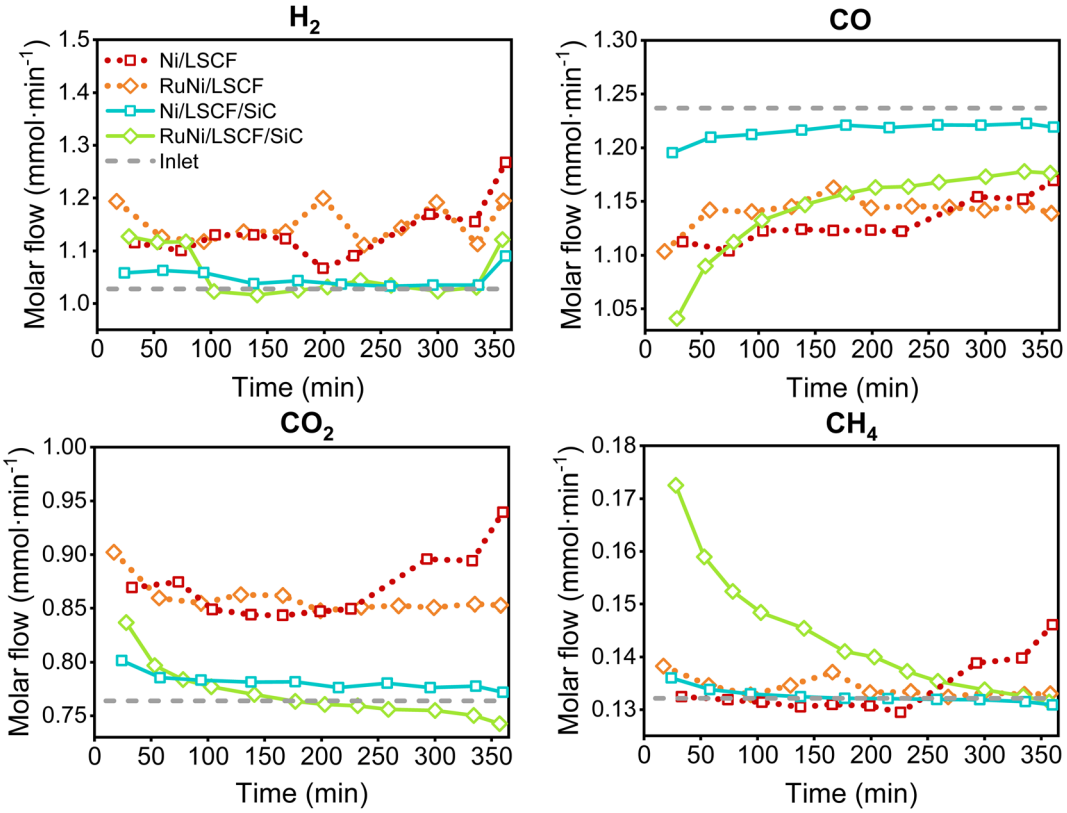

Fig. 8 Molar flows of gaseous components at the inlet and outlet of the reactor during toluene reforming at 550 °C for 6 h.

may explain the differences in catalytic performance found between (Ru)Ni/LSCF and (Ru)Ni/LSCF/SiC. Moreover, it has been reported that SiC is quite inactive in WGS when compared with other mixed oxides,[18] which can also explain the low catalytic activity in WGS of the structured catalysts.

The morphology of the carbonaceous deposits was evaluated for the spent catalysts by SEM. The images are reported in Fig. 11S of the ESI† for both powders and structured catalysts. As observed after the pre-treatment (Fig. 7), filamentous carbon is generated, suggesting that the presence of toluene in the fed did not influence the morphology of the coke deposits. The same morphology was observed in these materials after toluene reforming when the pre-treatment was conducted in a H_2 atmosphere.[9] Its formation was associated with the reaction temperature used and some gaseous components present in the ex-model biomass atmosphere such as CO and CH_4.[9,50]

An average toluene conversion of 54% for Ni/LSCF and 82% for RuNi/LSCF has been previously reached under the same reaction conditions when these catalysts were pre-treated in a H_2 atmosphere.[9] After the pre-treatment under a model ex-biomass gas atmosphere, both powders are still active in the WGS reaction while their catalytic activity in toluene reforming is quite poor. The catalytic activity in the WGS reaction exhibited for Ni/LSCF during tar reforming was mainly ascribed to the activity of the support (LSCF) and the activity in the tar reforming reaction was associated with the activity of the metallic Ni.[9] In order to verify that the catalytic activity in WGS evidenced for (Ru)Ni/LSCF in Fig. 8 comes from the activity of the support (LSCF), a comparison between the outlet molar flows of the bare LSCF and (Ru)Ni/LSCF is reported in Fig. 9S of the ESI.† The partial molar flows at the outlet of the reactor are quite similar for all the materials (Fig. 9S†), highlighting that the catalytic activity in the WGS reaction comes from the support. This fact indicates that the support remains active after the pre-treatment in the model ex-biomass gas atmosphere. Therefore, the deficient catalytic activity exhibited for Ni/LSCF in toluene reforming suggests that Ni particles become relatively inactive when the catalyst is pre-treated in the ex-biomass model gas atmosphere.

The whisker-like carbon deposits found at the surface of Ni/LSCF after the pre-treatment in the model ex-biomass gas atmosphere (see Fig. 7(a)) displayed a tip-growth mechanism because of the weak metal–support interaction. Some researchers reported an enhancement in the catalytic activity due to an increase in the metallic Ni surface as a consequence of this type of carbon growth mechanism. For instance, Souza *et al.*[55] pre-reduced Ni-based catalysts using a CH_4/O_2 atmosphere and compared their activity with those pre-treated under H_2. The formation of filamentous carbon during the pre-treatment in the CH_4/O_2 atmosphere encouraged the dispersion of Ni, leading to an improvement of the catalytic performance. He *et al.*[49] investigated the growth mechanism of the CNTs during steam reforming of toluene over Ni/α-Al_2O_3 and Ni/γ-Al_2O_3. Completely different catalytic behavior during toluene

reforming was observed for the two catalysts. This was ascribed to the type of growth mechanism of the carbon deposits. The catalytic performance was found to be better for the Ni/α-Al_2O_3 than for Ni/γ-Al_2O_3, which was ascribed to the improvement of the Ni dispersion by the tip growth mechanism of the CNTs. However, others reported a decline in the catalytic performance associated with the loss of the Ni–support interaction by detachment of Ni from the catalytic surface.[50] Therefore, this absence of activity in toluene reforming of the powders could be associated with the loss of the metal–support interaction by detachment of Ni from the catalytic support caused by the generation of the whisker carbon during the pre-treatment. Indeed, the tip-growth mechanism leads to a new catalyst, mostly based on Ni deposited on filamentous carbon, which does not display catalytic activity in toluene reforming. Moreover, the presence of CO chemisorbed on Ni, or the high amount of coke accumulated at the surface of the Ni/LSCF could also decrease the accessibility of Ni, decreasing its activity. The addition of Ru over Ni/LSCF improves the toluene conversion, although this conversion is still low (19%) and it is mainly converted in benzene (selectivity to benzene of 10%). In a previous study, better dispersion of the metals caused by a stronger metal–perovskite interaction has been observed by TEM for RuNi/LSCF with respect to Ni/LSCF (see Fig. 10S†).[9] This improvement in the metal dispersion owing to the presence of Ru could explain the slightly better catalytic performance of RuNi/LSCF in toluene reforming compared to Ni/LSCF. Moreover, the resistance to coke formation is also enhanced by the presence of Ru, making a high number of Ni active sites available.

Generally, the catalytic structuration improved the efficiency in tar removal. A decrease in the amount of coke and an increase in toluene conversion were found when the catalysts were structured on SiC extrudates. Several studies have reported an improvement in the catalytic activity when SiC was used as a carrier material or support. The high thermal conductivity of SiC inhibits the cold/hot spots and thermal shocks caused in the catalytic surface by the exothermicity or endothermicity of the reactions, keeping it under quasi isothermal conditions.[28,56,57] This avoids sintering and reduces the formation of coke deposits at the surface of the catalyst. Tar reforming and CO methanation are respectively highly endothermic and exothermic reactions and can lead to the formation of cold/hot spots in the catalytic surface, promoting the formation of coke and sintering of the metal particles. Therefore, the improvement in the activity in toluene reforming by structuring the catalysts highlights that the use of SiC as a carrier material helps to mitigate the uneven heat distribution at the surface of the catalyst and, thus, improves the resistance to coke formation. Moreover, the strong NiO–SiC interaction induced by the structuration might also influence the efficiency in tar removal. As previously discussed, this strong interaction favors the base-growth mechanism of the carbon deposits generated at the surface of the structured catalysts after the pre-treatment, hindering the detachment of Ni from the support. Moreover, it has been reported that a strong NiO–support interaction inhibits Ni agglomeration by limiting the migration of Ni particles on the surface of the support.[42] Thus, the presence of NiO having strong interaction with the SiC achieved through the structuration might limit or inhibit: (i) the detachment of Ni from the support/carrier material during the pre-treatment under the ex-biomass model gas atmosphere, since the base-growth mechanism prevails over the tip-growth one and (ii) the sintering of Ni that can occur during the pre-treatment or the catalytic test.

4. Conclusions

For the industrial use of (Ru)Ni/LSCF catalysts as secondary catalysts in a small biomass gasification installation, their catalytic structuration on SiC extrudates was conducted. The pre-treatment using a model ex-biomass gas atmosphere was performed for all the catalysts to verify its efficiency in reducing NiO/RuO_2 species. The influence of the structuration and pre-treatment on the physicochemical properties and catalytic activity of the catalysts in toluene reforming was investigated and the results were compared with those of the respective powders.

The catalytic structuration modified the crystalline phases and the interaction of them with the SiC. The formation of the individual oxides and silicates instead of the perovskite mixed oxide was favored through catalytic structuration. The metal–support–SiC interaction was also changed when the catalysts were structured on SiC. The phases deposited on SiC had stronger interaction with SiC than the one observed in the powders. Although filamentous carbon is formed during the pre-treatment, both systems, powders and structured catalysts, were successfully reduced using a model ex-biomass atmosphere. The catalytic activity in toluene reforming was quite poor for the powders due to the high deactivation by coke and the detachment of Ni from the support caused by the pre-treatment. Generally, an improvement in the catalytic performance in toluene reforming was attained when the catalysts were structured on SiC. The structuration improved the resistance to coke formation, likely due to the high conductivity of SiC, which allowed an even temperature distribution in the catalytic surface. Besides, the strong Ni–SiC interaction reached through the structuration hindered the detachment of Ni from the surface. Therefore, it can be concluded that structuration of catalysts on SiC extrudates is a promising strategy for the preparation of secondary catalysts that will be further used for tar removal in a downstream reactor during biomass gasification.

Conflicts of interest

There are no conflicts to declare.

Acknowledgements

This work was conducted in the framework of Efficient Use of Biomass for Low Emissions Production of Renewable Energy and Biotechnological Valuable Products (EBIPREP) Project of the INTERREG IV Rhin Superior Program, co-financed by

FEDER funds from the European Union – grant no. 3.6. The authors acknowledge SICAT for supplying the SiC extrudates.

References

1 X. Chen, X. Ma and X. Peng, Role of Filamentous Coke in Deactivation of Ni/Bio-Char Catalyst during Dry Reforming of Non-Oxygenates Tar, *J. Anal. Appl. Pyrolysis*, 2021, **159**, 105314, DOI: 10.1016/j.jaap.2021.105314.

2 S. Kawi, J. Ashok, N. Dewangan, S. Pati and C. Junmei, Recent Advances in Catalyst Technology for Biomass Tar Model Reforming: Thermal, Plasma and Membrane Reactors, *Waste Biomass Valorization*, 2022, **13**, 1–30, DOI: 10.1007/s12649-021-01446-6.

3 V. Claude, C. Courson, M. Köhler and S. D. Lambert, Overview and Essentials of Biomass Gasification Technologies and Their Catalytic Cleaning Methods, *Energy Fuels*, 2016, **30**, 8791–8814, DOI: 10.1021/acs.energyfuels.6b01642.

4 Y. Shen and K. Yoshikawa, Recent Progresses in Catalytic Tar Elimination during Biomass Gasification or Pyrolysis - A Review, *Renewable Sustainable Energy Rev.*, 2013, **21**, 371–392, DOI: 10.1016/j.rser.2012.12.062.

5 Y. A. Situmorang, Z. Zhao, A. Yoshida, A. Abudula and G. Guan, Small-Scale Biomass Gasification Systems for Power Generation (<200 KW Class): A Review, *Renewable Sustainable Energy Rev.*, 2020, **117**, 109486, DOI: 10.1016/j.rser.2019.109486.

6 E. Bocci, M. Sisinni, M. Moneti, L. Vecchione, A. Di Carlo and M. Villarini, State of Art of Small Scale Biomass Gasification Power Systems: A Review of the Different Typologies, *Energy Procedia*, 2014, **45**, 247–256, DOI: 10.1016/j.egypro.2014.01.027.

7 A. A. Ahmad, N. A. Zawawi, F. H. Kasim, A. Inayat and A. Khasri, Assessing the Gasification Performance of Biomass: A Review on Biomass Gasification Process Conditions, Optimization and Economic Evaluation, *Renewable Sustainable Energy Rev.*, 2016, **53**, 1333–1347, DOI: 10.1016/j.rser.2015.09.030.

8 R. Amin, B. S. Liu, Y. C. Zhao and Z. B. Huang, Hydrogen Production by Corncob/CO2 Dry Reforming over CeO2 Modified Ni-Based MCM-22 Catalysts, *Int. J. Hydrogen Energy*, 2016, **41**, 12869–12879, DOI: 10.1016/j.ijhydene.2016.05.233.

9 L. Jurado, V. Papaefthimiou, S. Thomas and A.-C. Roger, Upgrading Syngas from Wood Gasification through Steam Reforming of Tars over Highly Active Ni-Perovskite Catalysts at Relatively Low Temperature, *Appl. Catal., B*, 2021, **299**, 120687, DOI: 10.1016/j.apcatb.2021.120687.

10 L. Jurado, V. Papaefthimiou, S. Thomas and A. Roger, Low Temperature Toluene and Phenol Abatement as Tar Model Molecules over Ni-Based Catalysts: Influence of the Support and the Synthesis Method, *Appl. Catal., B*, 2021, **297**, 120479, DOI: 10.1016/j.apcatb.2021.120479.

11 L. Garcia, M. L. Salvador, J. Arauzo and R. Bilbao, Influence of Catalyst Weight/Biomass Flow Rate Ratio on Gas Production in the Catalytic Pyrolysis of Pine Sawdust at Low Temperatures, *Ind. Eng. Chem. Res.*, 1998, **37**, 3812–3819, DOI: 10.1021/ie9801960.

12 Y. Tanaka, T. Yamaguchi, K. Yamasaki, A. Ueno and Y. Kotera, Catalyst for Steam Gasification of Wood to Methanol Synthesis Gas, *Ind. Eng. Chem. Prod. Res. Dev.*, 1984, **23**, 225–229, DOI: 10.1021/i300014a009.

13 L. Garcia, M. L. Salvador, R. Bilbao and J. Arauzo, Influence of Calcination and Reduction Conditions on the Catalyst Performance in the Pyrolysis Process of Biomass, *Energy Fuels*, 1998, **12**, 139–143, DOI: 10.1021/ef970097j.

14 L. García, M. L. Salvador, J. Arauzo and R. Bilbao, Catalytic Steam Gasification of Pine Sawdust. Effect of Catalyst Weight/Biomass Flow Rate and Steam/Biomass Ratios on Gas Production and Composition, *Energy Fuels*, 1999, **13**, 851–859, DOI: 10.1021/ef980250p.

15 D. Carmello, A. Marsella, P. Forzatti, E. Tronconi and G. Groppi, Metallic Monolith Catalyst Support for Selective Gas Phase Reactions in Tubular Fixed Bed Reactors, *US Pat.*, US7678343, 2000.

16 M. Frey, T. Romero, A. C. Roger and D. Edouard, An Intensification of the CO_2 Methanation Reaction: Effect of Carbon Nanofiber Network on the Hydrodynamic, Thermal and Catalytic Properties of Reactors Filled with Open Cell Foams, *Chem. Eng. Sci.*, 2019, **195**, 271–280, DOI: 10.1016/j.ces.2018.11.028.

17 D. L. Nguyen, P. Leroi, M. J. Ledoux and C. Pham-Huu, Influence of the Oxygen Pretreatment on the CO_2 Reforming of Methane on Ni/β-SiC Catalyst, *Catal. Today*, 2009, **141**, 393–396, DOI: 10.1016/j.cattod.2008.10.019.

18 S. M. Kim and S. I. Woo, Sustainable Production of Syngas from Biomass-Derived Glycerol by Steam Reforming over Highly Stable Ni/SiC, *ChemSusChem*, 2012, **5**, 1513–1522, DOI: 10.1002/cssc.201100821.

19 J. M. García-Vargas, J. L. Valverde, A. de Lucas-Consuegra, B. Gómez-Monedero, P. Sánchez and F. Dorado, Precursor Influence and Catalytic Behaviour of Ni/CeO_2 and Ni/SiC Catalysts for the Tri-Reforming Process, *Appl. Catal., A*, 2012, **431–432**, 49–56, DOI: 10.1016/j.apcata.2012.04.016.

20 C. Li, H. Xu, S. Hou, J. Sun, F. Meng, J. Ma and N. Tsubaki, SiC Foam Monolith Catalyst for Pressurized Adiabatic Methane Reforming, *Appl. Energy*, 2013, **107**, 297–303, DOI: 10.1016/j.apenergy.2013.02.039.

21 J. M. García-Vargas, J. L. Valverde, J. Díez, P. Sánchez and F. Dorado, Influence of Alkaline and Alkaline-Earth Cocations on the Performance of Ni/β-SiC Catalysts in the Methane Tri-Reforming Reaction, *Appl. Catal., B*, 2014, **148–149**, 322–329, DOI: 10.1016/j.apcatb.2013.11.013.

22 J. M. García-Vargas, J. L. Valverde, J. Díez, P. Sánchez and F. Dorado, Preparation of Ni–Mg/β-SiC Catalysts for the Methane Tri-Reforming: Effect of the Order of Metal Impregnation, *Appl. Catal., B*, 2015, **164**, 316–323, DOI: 10.1016/j.apcatb.2014.09.044.

23 A. R. Kim, H. Y. Lee, D. H. Lee, B.-W. Kim, C.-H. Chung, D. J. Moon, E. J. Jang, C. Pang and J. W. Bae, Combined Steam and CO_2 Reforming of CH_4 on $LaSrNiO_x$ Mixed Oxides Supported on Al_2O_3 -Modified SiC Support, *Energy Fuels*, 2015, **29**, 1055–1065, DOI: 10.1021/ef501938v.

24 Q. Wei, G. Yang, Y. Yoneyama, T. Vitidsant and N. Tsubaki, Designing a Novel Ni–Al_2O_3–SiC Catalyst with a Stereo Structure for the Combined Methane Conversion Process to Effectively Produce Syngas, *Catal. Today*, 2016, **265**, 36–44, DOI: 10.1016/j.cattod.2015.08.029.

25 Q. Wei, G. Yang, X. Gao, N. Yamane, P. Zhang, G. Liu and N. Tsubaki, Ni/Silicalite-1 Coating Being Coated on SiC Foam: A Tailor-Made Monolith Catalyst for Syngas Production Using a Combined Methane Reforming Process, *Chem. Eng. J.*, 2017, **327**, 465–473, DOI: 10.1016/j.cej.2017.06.109.

26 H. Nam, Z. Wang, S. R. Shanmugam, S. Adhikari and N. Abdoulmoumine, Chemical Looping Dry Reforming of Benzene as a Gasification Tar Model Compound with Ni- and Fe-Based Oxygen Carriers in a Fluidized Bed Reactor, *Int. J. Hydrogen Energy*, 2018, **43**, 18790–18800, DOI: 10.1016/j.ijhydene.2018.08.103.

27 Z. Zhang, G. Zhao, G. Bi, Y. Guo and J. Xie, Monolithic SiC-Foam Supported Ni-La2O3 Composites for Dry Reforming of Methane with Enhanced Carbon Resistance, *Fuel Process. Technol.*, 2021, **212**, 106627, DOI: 10.1016/j.fuproc.2020.106627.

28 Z. Zhang, G. Zhao, W. Li, J. Zhong and J. Xie, Key Properties of Ni/$CeAlO_3$-Al_2O_3/SiC-Foam Catalysts for Biogas Reforming: Enhanced Stability and CO_2 Activation, *Fuel*, 2022, **307**, 121799, DOI: 10.1016/j.fuel.2021.121799.

29 M. Frey, T. Romero, A. C. Roger and D. Edouard, Open Cell Foam Catalysts for CO_2 Methanation: Presentation of Coating Procedures and In Situ Exothermicity Reaction Study by Infrared Thermography, *Catal. Today*, 2016, **273**, 83–90, DOI: 10.1016/j.cattod.2016.03.016.

30 A. Waldvogel, Mise au point d'un catalyseur performant pour la chaîne de procédé Power-to-Methane et étude cinétique, *Thèse Catalyse*, Université de Strasbourg, 2017, Français, NNT : 2017STRAF077, tel-01881957.

31 P. Nguyen and C. Pham, Innovative Porous SiC-Based Materials: From Nanoscopic Understandings to Tunable Carriers Serving Catalytic Needs, *Appl. Catal., A*, 2011, **391**, 443–454, DOI: 10.1016/j.apcata.2010.07.054.

32 B. De Tymowski, Y. Liu, C. Meny, C. Lefèvre, D. Begin, P. Nguyen, C. Pham, D. Edouard, F. Luck and C. Pham-Huu, Co-Ru/SiC Impregnated with Ethanol as an Effective Catalyst for the Fischer-Tropsch Synthesis, *Appl. Catal., A*, 2012, **419–420**, 31–40, DOI: 10.1016/j.apcata.2012.01.004.

33 P. Avila, M. Montes and E. E. Miró, Monolithic Reactors for Environmental Applications: A Review on Preparation Technologies, *Chem. Eng. J.*, 2005, **109**, 11–36, DOI: 10.1016/j.cej.2005.02.025.

34 L. Huang, M. Bassir and S. Kaliaguine, Reducibility of Co^{3+} in Perovskite-Type $LaCoO_3$ and Promotion of Copper on the Reduction of Co^{3+} in Perovskite-Type Oxides, *Appl. Surf. Sci.*, 2005, **243**, 360–375, DOI: 10.1016/j.apsusc.2004.09.079.

35 J. Deng, H. Dai, H. Jiang, L. Zhang, G. Wang, H. He and A. U. Chak Tong, Hydrothermal Fabrication and Catalytic Properties of $La_{1-x}Sr_xM_{1-y}Fe_yO_3$ (M = Mn, Co) That Are Highly Active for the Removal of Toluene, *Environ. Sci. Technol.*, 2010, **44**, 2618–2623, DOI: 10.1021/es9031997.

36 P. H. T. Ngamou and N. Bahlawane, Influence of the Arrangement of the Octahedrally Coordinated Trivalent Cobalt Cations on the Electrical Charge Transport and Surface Reactivity, *Chem. Mater.*, 2010, **22**, 4158–4165, DOI: 10.1021/cm1004642.

37 T. Zhao, J. Zhao, X. Tao, H. Yu, M. Li, J. Zeng and H. Wang, Highly Active and Thermostable Submonolayer La(NiCo)OΔ Catalyst Stabilized by a Perovskite $LaCrO_3$ Support, *Commun. Chem.*, 2022, **5**, 70, DOI: 10.1038/s42004-022-00686-4.

38 B. de Tymowski, Y. Liu, C. Meny, C. Lefèvre, D. Begin, P. Nguyen, C. Pham, D. Edouard, F. Luck and C. Pham-Huu, Co–Ru/SiC Impregnated with Ethanol as an Effective Catalyst for the Fischer–Tropsch Synthesis, *Appl. Catal., A*, 2012, **419–420**, 31–40, DOI: 10.1016/j.apcata.2012.01.004.

39 J. A. Díaz, M. Calvo-Serrano, A. R. De La Osa, A. M. García-Minguillán, A. Romero, A. Giroir-Fendler and J. L. Valverde, β-Silicon Carbide as a Catalyst Support in the Fischer-Tropsch Synthesis: Influence of the Modification of the Support by a Pore Agent and Acidic Treatment, *Appl. Catal., A*, 2014, **475**, 82–89, DOI: 10.1016/j.apcata.2014.01.021.

40 Z. F. Jiao, L. L. Dong, X. N. Guo, G. Q. Jin, X. Y. Guo and X. M. Wang, Methane Catalytic Combustion over Ni/SiC, Fe/SiC and Co/SiC Modified by $Zr_{0.5}Ce_{0.5}O_2$ Solid Solution, *Acta Phys.-Chim. Sin.*, 2014, **30**, 1941–1946, DOI: 10.3866/PKU.WHXB201408181.

41 S. He, Q. Jing, W. Yu, L. Mo, H. Lou and X. Zheng, Combination of CO_2 Reforming and Partial Oxidation of Methane to Produce Syngas over Ni/SiO_2 Prepared with Nickel Citrate Precursor, *Catal. Today*, 2010, **148**, 130–133, DOI: 10.1016/j.cattod.2009.03.009.

42 P. F. Guo, G. Q. Jin, C. X. Guo, Y. Y. Wang, X. L. Tong and X. Y. Guo, Effects of Yb_2O_3 Promotor on the Performance of Ni/SiC Catalysts in CO_2 Reforming of CH_4, *J. Fuel Chem. Technol.*, 2014, **42**, 719–726, DOI: 10.1016/s1872-5813(14)60033-5.

43 H. J. Zhan, X. Y. Shi, X. Huang and N. Zhao, Highly Coke-Resistant Ordered Mesoporous Ni/SiC with Large Surface Areas in CO_2 Reforming of CH_4, *J. Fuel Chem. Technol.*, 2019, **47**, 942–948, DOI: 10.1016/s1872-5813(19)30039-8.

44 G. Jin, F. Gu, Q. Liu, X. Wang, L. Jia and G. Xu, Highly Stable Ni/SiC Catalyst Modified by Al_2O_3 for CO Methanation Reaction, *RSC Adv.*, 2016, **6**, 9631–9639, DOI: 10.1039/c5ra19940a.

45 O. Clause, L. Bonneviot and M. Che, Effect of the Preparation Method on the Thermal Stability of Silica-Supported Nickel Oxide as Studied by EXAFS and TPR Techniques, *J. Catal.*, 1992, **138**, 195–205, DOI: 10.1016/0021-9517(92)90017-C.

46 N. Gao, J. Salisu, C. Quan and P. Williams, Modified Nickel-Based Catalysts for Improved Steam Reforming of Biomass Tar: A Critical Review, *Renewable Sustainable Energy Rev.*, 2021, **145**, 111023, DOI: 10.1016/j.rser.2021.111023.

47 A. Gohier, C. P. Ewels, T. M. Minea and M. A. Djouadi, Carbon Nanotube Growth Mechanism Switches from Tip- to Base-Growth with Decreasing Catalyst Particle Size, *Carbon*, 2008, **46**, 1331–1338, DOI: 10.1016/j.carbon.2008.05.016.

48 R. T. K. Baker, Catalytic Growth of Carbon Filaments, *Carbon*, 1989, **27**, 315–323, DOI: **10.1016/0008-6223(89)90062-6**.

49 L. He, S. Hu, L. Jiang, G. Liao, X. Chen, H. Han, L. Xiao, Q. Ren, Y. Wang, S. Su, *et al.*, Carbon Nanotubes Formation and Its Influence on Steam Reforming of Toluene over Ni/Al_2O_3 Catalysts: Roles of Catalyst Supports, *Fuel Process. Technol.*, 2018, **176**, 7–14, DOI: **10.1016/j.fuproc.2018.03.007**.

50 A. Łamacz, P. Babiński and G. Łabojko, The Impact of Components of Synthesis Gas from Coal Gasification on Conversion of Model Tar Compounds over $Ni/CeZrO_2$ Catalyst, *Fuel*, 2019, **236**, 984–992, DOI: **10.1016/j.fuel.2018.09.075**.

51 N. Charisiou, S. Douvartzides, G. Siakavelas, L. Tzounis, V. Sebastian, V. Stolojan, S. Hinder, M. Baker, K. Polychronopoulou and M. Goula, The Relationship between Reaction Temperature and Carbon Deposition on Nickel Catalysts Based on Al_2O_3, ZrO_2 or SiO_2 Supports during the Biogas Dry Reforming Reaction, *Catalysts*, 2019, **9**, 676, DOI: **10.3390/catal9080676**.

52 W. Fang, C. Pirez, P. L. Dhepe, F. Dumeignil and L. Jalowiecki-duhamel, Ce – Ni Mixed Oxide as Efficient Catalyst for H2 Production and Nanofibrous Carbon Material from Ethanol in the Presence of Water, *RSC Adv.*, 2012, 9626–9634, DOI: **10.1039/c2ra21701e**.

53 M. Koike, D. Li, H. Watanabe, Y. Nakagawa and K. Tomishige, Comparative Study on Steam Reforming of Model Aromatic Compounds of Biomass Tar over Ni and Ni-Fe Alloy Nanoparticles, *Appl. Catal., A*, 2015, **506**, 151–162, DOI: **10.1016/j.apcata.2015.09.007**.

54 P. Panagiotopoulou, D. I. Kondarides and X. E. Verykios, Selective Methanation of CO over Supported Ru Catalysts, *Appl. Catal., B*, 2009, **88**, 470–478, DOI: **10.1016/j.apcatb.2008.10.012**.

55 M. D. M. V. M. Souza, L. Clavé, V. Dubois, C. A. C. Perez and M. Schmal, Activation of Supported Nickel Catalysts for Carbon Dioxide Reforming of Methane, *Appl. Catal., A*, 2004, **272**, 133–139, DOI: **10.1016/j.apcata.2004.05.026**.

56 G. Lezcano, V. K. Velisoju, S. R. Kulkarni, A. Ramirez and P. Castaño, Engineering Thermally Resistant Catalytic Particles for Oxidative Coupling of Methane Using Spray-Drying and Incorporating SiC, *Ind. Eng. Chem. Res.*, 2021, **60**, 18770–18780, DOI: **10.1021/acs.iecr.1c02802**.

57 G. Lezcano, S. R. Kulkarni, V. K. Velisoju, V. E. Musteata, I. Hita, A. Ramirez, A. Dikhtiarenko, J. Gascon and P. Castaño, Effect of the Particle Blending-Shaping Method and Silicon Carbide Crystal Phase for $Mn\text{-}Na\text{-}W/SiO_2$-SiC Catalyst in Oxidative Coupling of Methane, *Mol. Catal.*, 2022, **527**, 112399, DOI: **10.1016/j.mcat.2022.112399**.